Cloud-Top Height Variability Associated with Equatorial Kelvin Waves in the Tropical Tropopause Layer during the Mirai Indian Ocean cruise for the Study of the MJO-Convection Onset (MISMO) Campaign

Junko Suzuki[1], Masatomo Fujiwara[2], Atsushi Hamada[3], Yoichi Inai[4], Jun Yamaguchi[5], Ryuichi Shirooka[1], Fumio Hasebe[2], and Toshiaki Takano[6]

[1]*Japan Agency for Marine-Earth Science and Technology, Yokosuka, Japan*
[2]*Graduate School Environmental Science, Hokkaido University, Sapporo, Japan*
[3]*Research Institute for Humanity and Nature, Kyoto, Japan*
[4]*Graduate School of Environmental Studies, Nagoya University, Nagoya, Japan*
[5]*Japan Aerospace Exploration Agency, Tsukuba, Japan*
[6]*Graduate School Engineering, Chiba University, Chiba, Japan*

Abstract

Cloud-top height (CTH) variability in the tropical tropopause layer (TTL) in association with equatorial Kelvin waves is investigated using a new CTH dataset based on MTSAT-1R geostationary satellite measurements with a statistical look-up table constructed based on CloudSat measurements. We focus on a case in the tropical Indian Ocean during October−December 2006, when shipboard radiosonde, TTL water vapor, and 95-GHz cloud radar measurements were taken during the Mirai Indian Ocean cruise for the Study of the MJO-convection Onset (MISMO) field campaign. At 10−15 km, the satellite-based CTH data agree well with the radar echo top heights from shipboard radar reflectivity data. During the MISMO campaign, cloud frequency was suppressed in the warm phase of equatorial Kelvin waves propagating in the TTL. The suppressed-cloud region moves eastward to the western Pacific together with Kelvin waves. We found that changes in CTH occurrence frequency over the vessel in association with Kelvin waves are much greater than those associated with the diurnal cycle. It is expected that the phase of equatorial Kelvin waves is important for the intraseasonal variabilities of both the radiative budget of the tropical atmosphere and water vapor transport in the TTL.

1. Introduction

Clouds of various types are frequent in the tropical tropopause layer (TTL) and play a critical role in the dehydration of the stratosphere (Fueglistaler et al. 2009) and troposphere-to-stratosphere transport by modulating the local radiative heat balance (Corti et al. 2006). These clouds in the TTL may also contribute to the radiative budget of the tropical atmosphere (e.g., McFarquhar et al. 2000). The variability of TTL clouds depends on cloud microphysics (Peter et al. 2006), cloud dynamics (Boehm et al. 1999), and large-scale dynamics (Fujiwara et al. 2009). On synoptic to subseasonal time scales, equatorial Kelvin waves are one of the most influential disturbances in the TTL (Suzuki and Shiotani 2008; Suzuki et al. 2010), significantly affecting the cirrus variability there (Boehm and Verlinde 2000; Immler et al. 2008; Fujiwara et al. 2009).

Ground-based lidar and cloud radar measurements are useful for studying clouds in the TTL at high temporal and vertical resolutions; however, it is difficult to measure the horizontal distribution of cloud layers. Satellite-borne lidar and radar measurements can detect their horizontal variability; however, with polar-orbiting satellites, it is difficult to detect the temporal evolution of clouds at sub-diurnal time scales. Infrared brightness temperature (Tb) data from geostationary satellites have been used to estimate the cloud top height in the tropics over a wide area at a high temporal resolution. However, it is known that, even for deep convective clouds, the estimated cloud top height (CTH) has negative biases compared with lidar measurements (Sherwood et al. 2004).

Recently, Hamada and Nishi (2010) (hereafter referred to as HN10) constructed a look-up table for estimating the CTH by regressing the echo-top heights measured with the CloudSat satellite cloud radar over Tb measurements at 10.8 μm and 12 μm with the geostationary satellite MTSAT-1R (covering ~70°E to ~150°W at a spatial resolution of 0.05°). The vertical temperature profiles, such as those obtained by radiosonde measurements and analysis data, were not used in constructing the table. This table can be adapted for all upper clouds, including non-precipitating clouds. This new CTH dataset makes it possible to monitor a particular cloud system over a time interval of 1 hour.

In this paper, we investigate a case of CTH variations associated with the passage of Kelvin waves in the TTL over the tropical Indian Ocean in October−December 2006. We use the CTH data based on HN10 taken during the Mirai Indian Ocean cruise for the Study of the MJO-convection Onset (MISMO) field experiment (Yoneyama et al. 2008). In this campaign, regular 3-hourly radiosoundings, 15 chilled-mirror hygrometer soundings, and continuous 95-GHz cloud radar measurements were conducted on the R/V *Mirai*. We first compare the satellite-based CTH data with the ship-borne cloud radar data. Then, we present the longitudinal and temporal variability of the CTH in association with Kelvin waves over the tropical Indian Ocean, where the Kelvin wave activity is highest in the TTL throughout the year (Suzuki and Shiotani 2008).

2. Data

During the MISMO field campaign from late October to early December 2006, the research vessel *Mirai* sailed in the Indian Ocean, between 4.0°S−3.0°N and 78.8°E−82.2°E during 22−27 October, stayed at 0°N, 80.5°E from 28 October to 21 November, and then cruised to Singapore at 103°E (Yoneyama et al. 2008). On the vessel, Vaisala RS92 radiosondes were launched regularly at 3-hourly intervals, and 15 Meteolabor Snow White chilled-mirror hygrometers were launched. The relative humidity over ice (RHi) in the upper troposphere was calculated using the frostpoint temperature measured with the Snow White hygrometers and the air temperature measured with the Vaisala RS80 radiosonde, which is directly attached to the Snow White hygrometers. The RHi measurements have an accuracy of ~1−2% in the tropical upper troposphere (Fujiwara et al. 2003). In addition, the

Corresponding author: Junko Suzuki, Japan Agency for Marine-Earth Science and Technology, 2-15 Natsushima-cho, Yokosuka 237-0061, Japan. E-mail: suzukij@jamstec.go.jp.

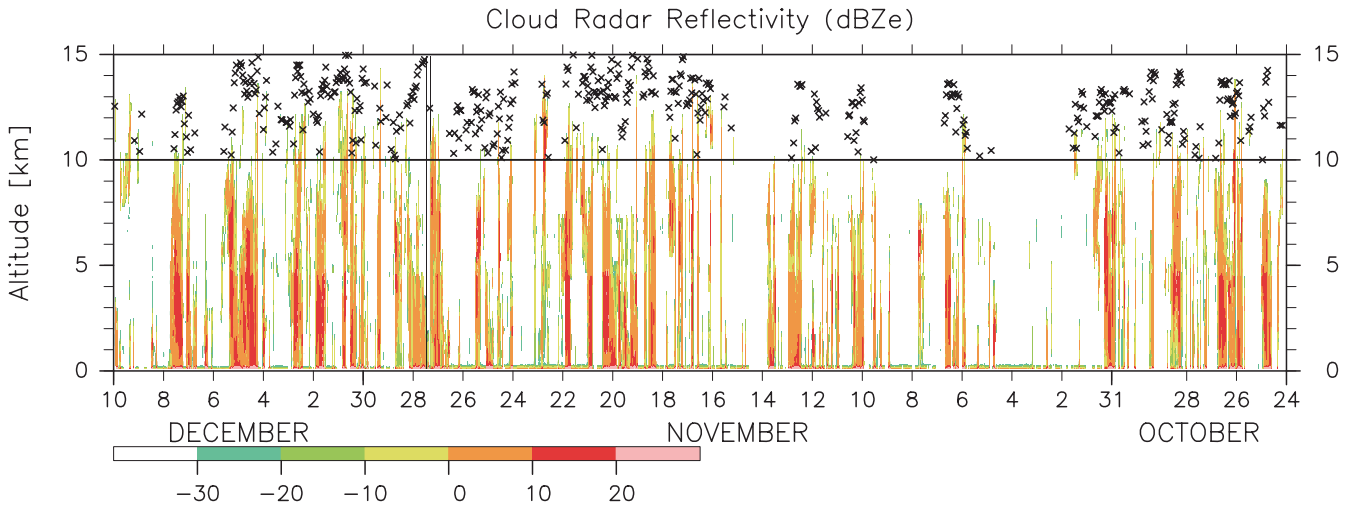

Fig. 1. Time-altitude distribution of radar reflectivity in units of dB (dBZe) over the R/V *Mirai* during the MISMO campaign between 24 October and 10 December 2006. Regions with ≥ −30 dBZe are colored. Missing measurements (around 27 November) are shown in dark gray. The location of the CTH using HN10 data at the grid point closest to the vessel at each time from 10 to 15 km is indicated by a black cross. The horizontal lines denote the 10-km height. Note that the time axis goes from right to left.

Frequency-Modulated, Continuous-Wave (FMCW), 95-GHz cloud-profiling radar "FALCON-I" of Chiba University was continuously operated on the vessel. For comparison with the CTH, the 95-GHz radar reflectivity in dB units was averaged for 60 minutes and for 183 m in the vertical direction, and the echo-top height was defined as the highest point where the echo reflectivity becomes −30 dBZe (Horie et al. 2000; Takano et al. 2008; Yamaguchi et al. 2009).

The CTH data based on HN10 are available over the area between ~70°E and ~160°E at a spatial resolution of 0.05° and a time resolution of 1 hour. The uncertainty of the CTH for upper tropospheric clouds is < 1 km at Tb < 240 K (above ~12.5 km), estimated from the standard deviation of the height difference between MTSAT-1R and CloudSat. We note that the uncertainty in CTH is large for thin cirrus clouds with an optical thickness of ≤ 2.5. We further define the CTH occurrence frequency (CTHOF) for each area of 9.95° latitude and 10° longitude centered at the location of the R/V *Mirai* in each vertical 0.5-km bin as N/N_{all}, where N_{all} is the number of total measurements (excluding missing measurements) in the area, and N is the number of grid points within that area where the CTH lies within the vertical bin. For instance, a CTHOF of 0.5 (= 50%) at 14.0 km means that a half of the 9.95° latitude-10° longitude area is occupied by clouds with tops between 13.75 and 14.25 km.

To investigate the relationship between the CTHOF variability and large-scale disturbances, we also analyzed temperature data at 150 hPa (~14.2 km) from the 6-hourly global operational analysis of the European Centre for Medium-Range Weather Forecasts (ECMWF), which were originally gridded at 1.125° in both longitude and latitude. We note that the time axes of Figs. 1, 2 and 4 go from right to left to show the zonal structure of eastward-moving disturbances; that is, equatorial Kelvin waves.

3. Results and discussion

Figure 1 shows the time-altitude distributions of the 95-GHz cloud radar reflectivity in units of dB (dBZe) over the R/V *Mirai* and the satellite-based CTH at the grid point nearest to the vessel. At 10−15 km, the satellite-based CTH corresponds well with the radar echo top height (the boundary between the colored and non-colored regions), although the location of the satellite observation grid may be up to ~4 km away from the vessel. A scatter plot for the satellite-based CTH versus the radar echo top height (not shown) indicates that there is ~1.47 km positive estimation bias for the satellite-based CTH and the standard deviation of the difference between the two heights is ~1.53 km. The two heights agree quite well from 26 October to 2 November and after 28 November, when the center and western side of large-scale convection passed over the vessel (Yoneyama et al. 2008). From 12 UTC 31 October to 1 November, the radar echo top height was around 10−13 km, showing cirrus cloud existence, as there was no echo below these signals. In some cases, the CTH was higher than the radar echo top. For example, during 10−11 November and 24−26 November, the CTH showed scatter over the vessel. This was caused by a remnant from an active convective system that came close to the vessel (confirmed by the MTSAT-1R data). At that time, the radar echo measurements were temporally disappearing.

Figure 2 shows the variability of the dynamical field measured with the regular radiosounding onboard the R/V *Mirai*. We observe that a zonal wind transition from easterly to westerly occurred at 16.5 km around 29 October down to 12 km around 3 November, when the isentropes showed downward motion from the tropopause to the mid-troposphere. This disturbance had a zonal wind amplitude of ~20 m s^{-1} at 14.5 km with a period of about two weeks (the period can be estimated from the half wavelength between the two zero curves in the zonal wind anomaly plot at ~14.5 km on 25 and 31 November). The vertical wavelength, λ_z, was estimated as ~8 km (the region from 14 km to 18 km on 1 November corresponds to half the wavelength). There was no substantial meridional-wind component corresponding to the zonal wind oscillation (not shown). These meteorological characteristics correspond to those of equatorial Kelvin waves. From the linear wave theory, the zonal phase speed was roughly estimated as 15 m s^{-1} and the zonal wavelength was roughly estimated as 1.8×10^4 km using the values, λ_z = 8 km, U = 0 m s^{-1} and N = 1.18×10^{-2} s^{-1}, where U is the background (constant) zonal wind and N is the Brunt-Väisälä (buoyancy) frequency around 14.2 km (~150 hPa). Figure 3 shows the longitude-time distribution of a temperature anomaly at 150 hPa (~14.2 km) using ECMWF data. The anomaly arises with respect to the temporal average between 22 October and 10 November. Figure 3 indicates a warm anomaly that moved eastward over the equatorial Indian Ocean from 31 October to 6 November at a zonal phase speed of ~15 m s^{-1}, coinciding with the descending isentropes observed over the R/V *Mirai* in Fig. 2 and corresponding to the value estimated using the linear wave theory.

To focus on the CTH variability associated with large-scale dynamics, we here use the CTHOF data defined in Section 2.

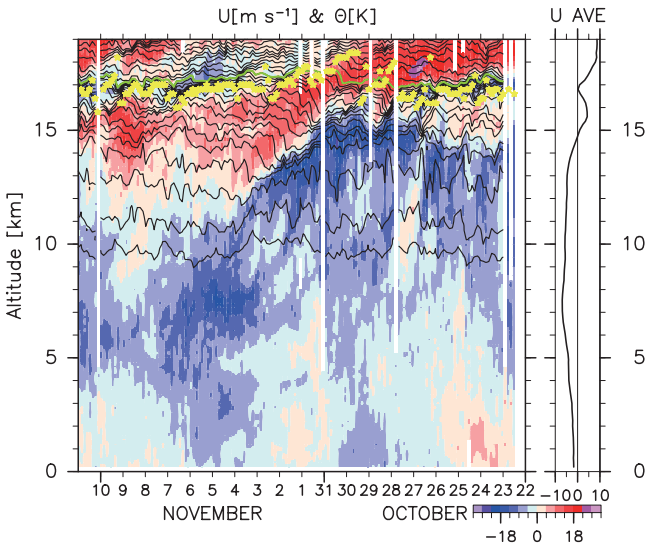

Fig. 2. (Left) Time-altitude distributions of zonal wind anomaly (colors) and potential temperature (contours: 3-K interval at 342−390 K, 6-K interval at 390−450 K and a light green line for 390 K) measured with the regular radiosounding onboard the vessel *Mirai*. Yellow stars indicate the location of the tropopause. The zonal wind anomaly is with respect to the temporal average between 22 October and 10 November. Note that the time axis goes from right to left. (Right) The average zonal wind profile during the period from 22 October and 11 November.

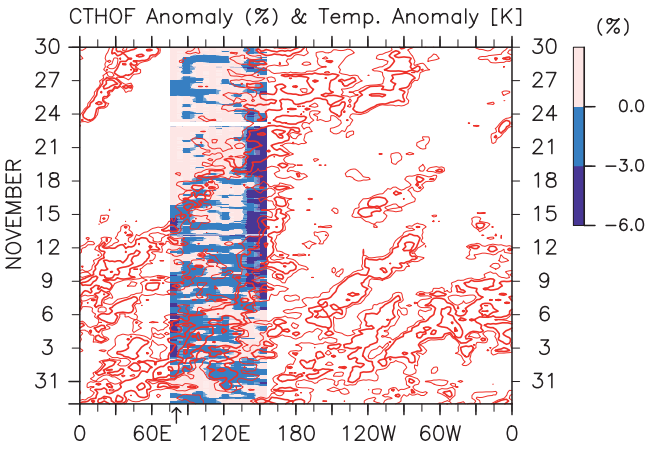

Fig. 3. Longitude-time distribution of the CTHOF anomaly at 14 km (colors, %) and the temperature anomaly at 150 hPa (contours: 0, 0.5, 1.5 and 2.5 K, only for warm anomalies). The anomaly is with respect to the temporal average from 22 October to 10 November. The arrow indicates the location of the vessel *Mirai* in Figs. 2 and 4.

Figure 4 shows the time-altitude distributions of CTHOF, potential temperature, and RHi over the R/V *Mirai*, focusing the period and altitude region on the zone where a packet of Kelvin waves is observed in Fig. 2. Large values of CTHOF are found at 13 km intermittently from 29 October to 2 November, suggesting that clouds with tops at 13 km were dominant during this period. After 31 October, there were fewer upper tropospheric clouds with tops reaching 15 km. The large CTHOF seen around 14 km on 1 November shows the cirrus clouds as described for Fig. 1.

The positive potential temperature anomaly in Fig. 4 corresponds to the warm phase of Kelvin waves. The largest potential temperature change was ~9 K at 15.5 km around 31 October, when the zonal wind anomaly was 0 m s^{-1}, as shown in Fig. 2. The phase difference between potential temperature and zonal wind satisfies the property of Kelvin wave. We observe in Fig. 4 that the 2.5% CTHOF regions descend with time, being co-located with positive potential temperature anomalies. Temperature inversions are observed along the line from 17.5 km on 29 October to 13 km on 2 November, coinciding with the ~0 K potential temperature anomaly and the 2.5% CTHOF region. This indicates that the lower boundary of the warm phase of Kelvin waves forms a temperature inversion layer, preventing moist convections and associated clouds from penetrating higher altitudes (estimated clouds types in Fig. 1). The diurnal changes of the CTHOF are largest at 13 km as ~3% and the peak of diurnal cycle is around 12 UTC (~17 local time).

Figure 4 also shows RHi profiles on 30 October and 1 November. On 30 October, very low RHi values were found around 15.5 km. These were located within the warm phase of Kelvin waves. On 1 November, the minimum RHi region had moved to 14−15.5 km, coincident with the positive temperature anomaly. The inversion layers are found at the lower edge of the very low RHi region in both profiles, and the high RHi region just below the inversions corresponds to the upper tropospheric clouds shown in the CTHOF data.

Figure 3 also shows the Hovmöller diagram of the CTHOF anomaly at 14 km. The negative CTHOF anomaly falling to −6% at 80.5°E from 31 October to 6 November coincides with the warm phase of the Kelvin waves (see also Fig. 4). The diurnal changes of the CTHOF at 14 km reached up to 1.5% in Fig. 4. Therefore, the CTHOF changes associated with the Kelvin waves were much larger than the diurnal changes in CTHOF at 80.5°E. The warm anomaly propagated further eastward and reached when the CTHOF fell to −6%. During 14−17 November, negative CTHOF anomalies are continuously observed around 150°E even after the warm phase of Kelvin waves has passed. This suggests that the cloud-top height does not recover even if the temperature becomes colder again. We also see that another warm anomaly at 80.5°E around 13−14 November propagated eastward and reached 150°E, where negative CTHOF anomalies coexisted. The CTHOF variability was weak at 120−140°E throughout this period; active convective clouds such as those reaching 14 km were rare in the region (not shown).

The two cases above suggest that TTL clouds are effectively

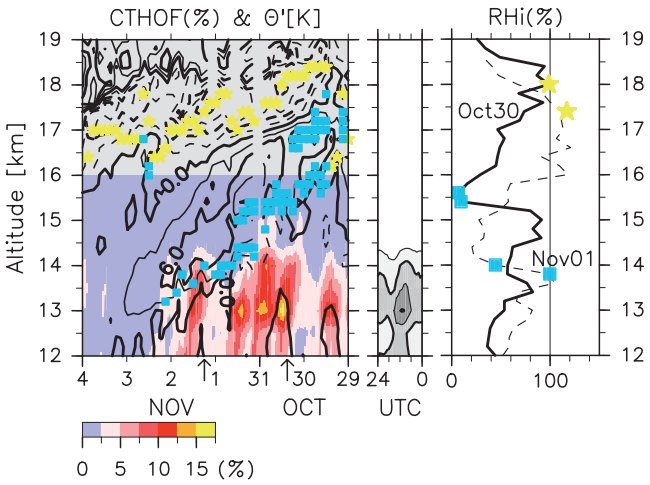

Fig. 4. (Left) Time-altitude distributions of the CTHOF (color, %) and potential temperature anomaly (contours: 3-K interval) from 29 October to 3 November. Yellow stars and blue squares indicate the locations of the tropopause and the lower boundary of the inversion layer (dT/dz > 0 K km^{-1}), respectively. The potential temperature anomaly is with respect to the temporal average between 22 October and 10 November. Note that the time axis goes from right to left. (Center) Time-altitude distribution of the CTHOF diurnal variation estimated between 22 October and 10 November (contours and shading are 2, 4, 6 and 8%). (Right) Profiles of relative humidity over ice (%) on 30 October (solid curve) and 1 November (dotted curve). Yellow stars and blue squares are the same as those in the left panel.

suppressed by the warm phases of equatorial Kelvin waves. Note that a small region about the ratio of the CTHOF at 14.5 km divided by the CTHOF at 13 km where the ratio was less than 0.4 propagated eastward with the warm phase of the Kelvin wave at 150 hPa (not shown). Therefore, the negative CTHOF anomaly at 14 km (N_{14km}/N_{all}; Fig. 3) was not caused by the increasing number of total clouds (N_{all}). At the same, the decrease in $N_{14.5km}$ is greater than in N_{13km}. Kelvin waves frequently propagate around 100 hPa (~16.5 km) in the eastern hemisphere but usually around 150 hPa (~14.2 km) and below in the western hemisphere (Suzuki et al. 2010). Therefore we expect that a large variability in the TTL clouds could be observed at higher altitudes in the eastern hemisphere than in the western hemisphere.

4. Conclusions

A new cloud-top height dataset prepared by HN10 and ship-borne cloud radar and radiosonde measurements during the MISMO campaign in the tropical Indian Ocean demonstrates the role of equatorial Kelvin waves in suppressing TTL cloud frequency. We further show that the region of decreased cloud occurrence moves eastward from ~80°E to ~150°E in association with the propagation of Kelvin waves. We also found that the variability in cloud occurrence at 80.5°E that was associated with the Kelvin waves is much larger than that associated with the diurnal cycle. We found that the cloud-top height in the tropics is controlled not only by lower tropospheric conditions such as the static stability and water vapor convergence but also by the equatorial Kelvin waves in the TTL. Modulated cloud-top heights could be found all over the equatorial region because Kelvin waves are ubiquitous throughout the equatorial region in the TTL (Suzuki and Shiotani 2008; Suzuki et al. 2010). The phase of large-scale dynamical waves in the TTL should be taken into account for the intraseasonal variability of the radiative budget of the tropical atmosphere and of water vapor transport into the stratosphere.

Acknowledgements

The authors express thanks to Dr. H. Okamoto of Kyushu University in obtaining the cloud radar data, to Dr. N. Nishi of Kyoto University for helpful discussions, and to two anonymous reviewers for helpful comments. The GFD-DENNOU Library was used to draw the figures.

References

Boehm, M. T., and J. Verlinde, 2000: Stratospheric influence on upper tropospheric tropical cirrus. *Geophys. Res. Lett.*, **27**, 3209−3212, doi:10.1029/2000GL011678.

Boehm, M. T., J. Verlinde, and T. P. Ackerman, 1999: On the maintenance of high tropical cirrus. *J. Geophys. Res.*, **104**, 24423−24433.

Corti, T., B. P. Luo, Q. Fu, H. Vömel, and T. Peter, 2006: The impact of cirrus clouds on tropical troposphere-to-stratosphere transport. *Atmos. Chem. Phys.*, **6**, 2539−2547.

Fueglistaler, S., A. E. Dessler, T. J. Dunkerton, I. Folkins, Q. Fu, and P. W. Mote, 2009: Tropical tropopause layer. *Rev. Geophys.*, **47**, RG1004, doi:10.1029/2008RG000267.

Fujiwara, M., S. Iwasaki, A. Shimizu, Y. Inai, M. Shiotani, F. Hasebe, I. Matsui, N. Sugimoto, H. Okamoto, N. Nishi, A. Hamada, T. Sakazaki, and K. Yoneyama, 2009: Cirrus observations in the tropical tropopause layer over the western Pacific. *J. Geophys. Res.*, **114**, D09304, doi:10.1029/2008JD011040.

Fujiwara, M., M. Shiotani, F. Hasebe, H. Vömel, S. J. Oltmans, P. W. Ruppert, T. Horinouchi, and T. Tsuda, 2003: Performance of the Meteolabor "Snow White" chilled-mirror hygrometer in the tropical troposphere: Comparisons with the Vaisala RS80 A/H-Humicap sensors. *J. Atmos. Oceanic Technol.*, **20**, 1534−1542.

Hamada, A., and N. Nishi, 2010: Development of a cloud-top height estimation method by geostationary satellite split-window measurements trained with CloudSat data. *J. Appl. Meteor. Climate*, (accepted).

Horie, H., T. Iguchi, H. Hanado, H. Kuroiwa, H. Okamoato, and H. Kumagai, 2000: Development of a 95-GHz airborne cloud profiling radar (SPIDER): Technical aspects. *IEICE Trans.*, **E83-B**, 2010−2020.

Immler, F., K. Kruger, M. Fujiwara, G. Verver, M. Rex, and O. Schrems, 2008: Correlation between equatorial Kelvin waves and the occurrence of extremely thin ice clouds at the tropical tropopause. *Atmos. Chem. Phys.*, **8**, 4019−4026.

McFarquhar, G. M., A. J. Heymsfield, J. Spinhirne, and B. Hart, 2000: Thin and subvisual tropopause tropical cirrus: Observations and radiative impacts. *J. Atmos. Sci.*, **57**, 1841−1853.

Peter, T., C. Marcolli, P. Spichtinger, T. Corti, M. B. Baker, and T. Koop, 2006: When dry air is too humid. *Science*, **314**, 1399−1402, doi:10.1126/science.1135199.

Sherwood, S. C., J.-H. Chae, P. Minnis, and M. McGill, 2004: Underestimation of deep convective cloud tops by thermal imagery. *Geophys. Res. Lett.*, **31**, L11102, doi:10.1029/2004GL019699.

Suzuki, J., and M. Shiotani, 2008: Space-time variability of equatorial Kelvin waves and intraseasonal oscillations around the tropical tropopause. *J. Geophys. Res.*, **113**, doi:10.1029/2007JD009456.

Suzuki, J., M. Shiotani, and N. Nishi, 2010: Lifetime and longitudinal variability of equatorial Kelvin waves around the tropical tropopause region. *J. Geophys. Res.*, **115**, doi:10.1029/2009JD012261.

Takano, T., J. Yamaguchi, H. Abe, K. Futaba, S. Yokote, Y. Kawamura, T. Takamura, H. Kumagai, Y. Ohno, Y. Nakanishi, and T. Nakajima, 2008: Development and performance of the millimeter-wave cloud profiling radar at 95 GHz: Sensitivity and spatial resolution. *IEEJ Trans. FM*, **128**, 257−262, doi:10.1541/ieejfms.128.257.

Yamaguchi, J., T. Takano, Y. Nakanishi, H. Abe, Y. Kawamura, S. Yokote, H. Kumagai, Y. Ohno, and H. Horie, 2009: Evaluation of radar reflectivity (Z) for FMCW millimeter-wave cloud radar "FALCON-I". *IEEJ Trans. FM*, **129**, 183−189, doi:10.1541/ieejfms.129.183.

Yoneyama, K., Y. Masumoto, Y. Kuroda, M. Katsumata, K. Mizuno, Y. N. Takayabu, M. Yoshizaki, A. Shareef, Y. Fujiyoshi, M. J. McPhaden, V. S. N. Murty, R. Shirooka, K. Yasunaga, H. Yamada, N. Sato, T. Ushiyama, Q. Moteki, A. Seiki, M. Fujita, K. Ando, H. Hase, I. Ueki, T. Horii, C. Yokoyama, and T. Miyakawa, 2008: MISMO field experiment in the equatorial Indian Ocean. *Bull. Amer. Meteor. Soc.*, **89**, 1889−1903, doi:10.1175/2008BAMS2519.1.

Manuscript received 8 June 2010, accepted 8 July 2010
SOLA: http://www.jstage.jst.go.jp/browse/sola/